
High-Angle-of-Attack Pneumatic Lag and Upwash Corrections for a Hemispherical Flow Direction Sensor

Stephen A. Whitmore, Jennifer Heeg, Terry J. Larson,
L.J. Ehernberger, Floyd W. Hagen, and Richard V. DeLeo

(NASA-TM-86790) HIGH-ANGLE-OF-ATTACK
PNEUMATIC LAG AND UPWASH CORRECTIONS FOR A
HEMISpherical FLOW DIRECTION SENSOR (NASA)
21 p Avail: NTIS HC A02/MF A01 CSCL 01D

N87-23616

H1/06 0076748
Unclassified

May 1987

High-Angle-of-Attack Pneumatic Lag and Upwash Corrections for a Hemispherical Flow Direction Sensor

Stephen A. Whitmore, Jennifer Heeg, Terry J. Larson, and L.J. Ehernberger
Ames Research Center, Dryden Flight Research Facility, Edwards, California
Floyd W. Hagen and Richard V. DeLeo
Rosemount, Inc., Eden Prairie, Minnesota

1987



National Aeronautics and
Space Administration
Ames Research Center
Dryden Flight Research Facility
Edwards, California 93523-5000

SUMMARY

As a part of the NASA F-14 high-angle-of-attack flight test program, a nose-mounted hemispherical flow direction sensor was calibrated against a fuselage-mounted movable-vane flow angle sensor. Significant discrepancies were found to exist in the angle-of-attack measurements.

This report describes a two-fold approach taken to resolve these discrepancies during subsonic flight. First, the sensing integrity of the isolated hemispherical sensor is established by wind tunnel data extending to an angle of attack of 60°. Second, two probable causes for the discrepancies, pneumatic lag and upwash, are examined. Methods of identifying and compensating for lag and upwash are presented.

The wind tunnel data verify that the isolated hemispherical sensor is sufficiently accurate for static conditions with angles of attack up to 60° and angles of sideslip up to 30°. Analysis of flight data for two high-angle-of-attack maneuvers establishes that pneumatic lag and upwash are highly correlated with the discrepancies between the hemispherical and vane-type sensor measurements.

INTRODUCTION

The F-14 high-angle-of-attack control system investigation at NASA Ames Research Center's Dryden Flight Research Facility provided an opportunity to investigate the measurement of air data at high angles of attack under both steady-state and maneuvering conditions. Angle-of-attack measurements obtained with a nose-mounted hemispherical sensor significantly differed from those obtained with a fuselage-mounted vane-type sensor (ref. 1). The discrepancies significantly exceeded 2° and contrasted greatly with the accuracy expected on the basis of previous wind tunnel and flight experience (refs. 2 to 4). An investigation to identify the sources of the discrepancies was initiated.

This report describes a two-fold approach taken to resolve these discrepancies. First, the sensing integrity of the isolated hemispherical sensor is established by wind tunnel data for static conditions. Angle-of-attack data are presented for static conditions for an angle-of-attack α range of $-4.0^\circ < \alpha < 60.0^\circ$, an angle-of-sideslip β range of $-30^\circ < \beta < 30^\circ$, and Mach numbers of 0.3, 0.4, and 0.5.

Second, the data discrepancy is significantly reduced by adjusting the nose-mounted sensor measurements for pneumatic lag and upwash. One technique for in-flight lag determination for a similar hemispherical flow direction sensor (ref. 5) employed small-amplitude flow angle oscillations that continued for several cycles. However, this approach is impractical at high angles of attack, so system identification and state reconstruction techniques were used to derive the appropriate adjustment factors for pneumatic lag and upwash. The techniques used to identify the adjustment factors are developed in more detail in the appendixes. Two flight maneuvers were used to perform this investigation. Flight data were obtained at Mach numbers of 0.60 and 0.85, $0^\circ < \alpha < 40.0^\circ$, $-10.0^\circ < \beta < 10.0^\circ$, and altitudes of 9145 and 11,890 m (30,000 and 39,000 ft).

NOMENCLATURE

b	bias term used in identifying pneumatic lag constant, kPa (lb/ft ²)
D	diameter of pressure transmission line, cm (in)
F	scale factor used in identifying pneumatic lag constant
K ₁	angle-of-attack proportionality factor
l	length of pressure transmission line, m (ft)
p(l, t)	pressure at transducer end of measurement device, kPa (lb/ft ²)
p _c (t)	pressure estimate resulting from complementary filter, kPa (lb/ft ²)
p _t (t)	pressure at free-stream end of measurement device, kPa (lb/ft ²)
p _o (t)	actual local pressure at the orifice, kPa (lb/ft ²)
p ₁	nose-mounted hemispherical sensor lower angle-of-attack pressure (fig. 1(b)), kPa (lb/ft ²)
p ₂	nose-mounted hemispherical sensor upper angle-of-attack pressure (fig. 1(b)), kPa (lb/ft ²)
p ₃	nose-mounted hemispherical sensor center pressure (fig. 1(b)), kPa (lb/ft ²)
p ₄	nose-mounted hemispherical sensor left angle-of-sideslip pressure (fig. 1(b)), kPa (lb/ft ²)
p ₅	nose-mounted hemispherical sensor right angle-of-sideslip pressure (fig. 1(b)), kPa (lb/ft ²)
q	free-stream dynamic pressure
T _g	lag geometry parameter
t	time, sec
V	sensor configuration enclosed volume, m ³ (ft ³)
α	angle of attack, deg
β	angle of sideslip, deg
Δt	measurement sample interval, sec
μ	dynamic viscosity of air, N/m-sec

τ_a time lag value of first-order lag model, sec

Subscripts

l value for local wind tunnel quantity

m quantity as measured by isolated hemispherical sensor in wind tunnel

DESCRIPTION OF SENSORS

The nose-mounted hemispherical head probe (test sensor) is used to derive flow angle, altitude, and airspeed quantities. Comparative data are measured by a fuselage-mounted movable-vane flow direction sensor (reference sensor) (fig. 1(a)).

Test Sensor

The nose-mounted test sensor uses pneumatic measurements to sense flow direction angles. The sensor as obtained from the manufacturer did not allow for angle-of-sideslip measurements, and it was modified for the F-14 high-angle-of-attack flight tests to provide angle-of-sideslip measurements in addition to angle-of-attack measurements. The modified hemispherical configuration senses pressures from five external orifices, arranged as depicted in figure 1(b). The angle of attack is calibrated to be a function of the five sensed pressures p_i ($i = 1$ to 5):

$$\alpha = \frac{K_1(p_1 - p_2)}{p_3 - (p_4 + p_5)/2} \quad (1)$$

where K_1 is the empirical proportionality factor, which is presented as a function of Mach number in reference 6. Pitch rate corrections were applied to the angle-of-attack data; however, no upwash corrections were applied prior to the identification of lag and upwash errors.

Accurate force-balance absolute-pressure transducers were used to measure the test sensor pressures. The largest uncertainties in these measurements were found to be ± 0.1436 kPa (± 3 lb/ft 2). All the pressures were recorded to a resolution of better than 0.01436 kPa (0.30 lb/ft 2). The accuracy and resolution representative of these pressure data are comparable to $\pm 1^\circ$ and 0.1° , respectively, in local angle of attack for the maneuver conditions described in this report.

Reference Sensor

Because of the modifications to the test sensor and the specific installation of the sensor on the aircraft, calibrations against a reference data source were performed to assess the accuracy of the installed configuration. The reference source, consisting of a calibrated NACA-standard boom with flow direction vanes only (fig. 1(c)) was mounted on the underside of the aircraft fuselage. Indicated values of local angle of attack were recorded to an accuracy of better than $\pm 0.1^\circ$.

TECHNIQUES FOR IDENTIFYING AND COMPENSATING FOR PNEUMATIC LAG ERRORS

Equation (1) uses nonlinear combinations of the five sensed pressures to compute angle of attack. When the sensed pressures include individual pneumatic lag errors, the nonlinear pressure combinations result in irregular angle-of-attack indications. Simply time-skewing the computed angle of attack will not account for the effects of pneumatic lag. The individual pressure measurements must be adjusted for lag errors, and the angle of attack must be recomputed using equation (1).

For this study, the dynamics of pneumatic lag are adequately described by a first-order model (ref. 7) of the form

$$\frac{dp(l, t)}{dt} + \frac{1}{\tau_a} p(l, t) = \frac{1}{\tau_a} p_t(t) \quad (2)$$

where l is the length of the pressure transmission line, t is time, $p(l, t)$ is the lagged pressure as recorded at the measurement transducer, $p_\infty(t)$ is the actual pressure at the orifice, and τ_a is the time lag value for the measurement configuration.

Using numerical integration, equation (2) may be converted to a digital compensator with $p(l, t)$ as the input and $p_\infty(t)$ as the output. Given the measured (lagged) pressure time history, this compensator may be used to compute an estimate of the pressure at the orifice. In this manner entire pressure measurement time histories may be adjusted for both phase lag and attenuation resulting from pneumatic lag. The conversion of equation (2) to a digital compensator is presented in appendix 1.

The time lag value is shown in reference 7 to be a function of both geometry and altitude. In practice the true geometry of the measurement configuration is seldom known, so the time lag value must be estimated by some empirical means. The state of the art in empirical parameter estimation is the maximum likelihood estimation technique. Using measured data and the model as presented in equation (2), we can estimate the value of τ_a by the maximum likelihood technique. Some specifics of the identification scheme are presented in appendix 2.

TECHNIQUE FOR IDENTIFYING AND COMPENSATING FOR UPWASH ERRORS

The test sensor data initially were not corrected for upwash. The following technique was used to determine the average test probe upwash adjustment factor: The free-stream angle of attack is estimated by merging several independent sources of trajectory data, both onboard and external to the aircraft, using a linearized Kalman filter. (The linearized Kalman filter technique used to merge the multiple data sources is described in appendix 3.) Once the free-stream angle of attack is estimated, the differences between the free-stream and test sensor angles of attack are computed for each time point in the maneuver. These differences are then normalized by the estimated free-stream angle of attack and averaged over time. The result is the upwash adjustment factor. To verify the upwash adjustment factors, they are compared with theoretical upwash adjustment factors computed by the Yaggy-Rogallo technique (ref. 8).

WIND TUNNEL AND FLIGHT DATA

Wind Tunnel Conditions

To evaluate the static accuracy of the isolated test (hemispherical) sensor, wind tunnel tests were conducted in the low-speed 7- by 17-ft test section of the Rosemount Transonic Wind Tunnel Facility (ref. 6). Test conditions are detailed in table 1.

Angle-of-attack errors at $\beta = 0^\circ$ and $-4.0^\circ < \alpha < 60.0^\circ$ are presented in figure 2, which shows the difference between the test sensor angle-of-attack measurement α_m and the free-stream angle of attack α_f as a function of free-stream angle of attack. The maximum error is slightly greater than 2° .

Figure 3 presents the angle-of-attack error as a function of free-stream angle of sideslip β_f for $\alpha_f = 0^\circ$ and 7.0° at Mach 0.3. The angle-of-sideslip excursion ranges from -30.0° to 30.0° . For $\alpha_f = 0^\circ$, the magnitude of the angle-of-attack error is slightly greater than 1° . For $\alpha_f = 7.0^\circ$, the angle-of-attack error is significant, with a maximum excursion of 3.0° . However, this maximum error occurs at very large angles of sideslip; for moderate angles of sideslip (in the range $-20.0^\circ < \beta_f < 20.0^\circ$), the angle-of-attack error is on the order of 1° .

Reference 1 reported angle-of-attack discrepancies exceeding 5° and, in the case of high-rate maneuvers, a hysteresis loop with an amplitude of more than 8° . In contrast, the wind tunnel data indicate that the steady-state errors in angle of attack are on the order of 1° . As a result, one must conclude that the errors are due to installation-dependent factors such as pneumatic lag and upwash.

Flight Maneuvers

To investigate the effects of lag and upwash, two maneuvers from the high-angle-of-attack program were chosen for use in identifying the angle-of-attack discrepancies. The maneuvers were chosen because they involved large excursions in angle of attack.

Maneuver I, a pullup maneuver, results in an angle-of-attack variation from 0° to 33.0° . The reference sensor angle of sideslip varies from -1.0° to 1.0° . Maneuver I was performed at an average Mach number of 0.85 and an average altitude of 11,890 m (39,000 ft) (fig. 4). Maneuver II, an alpha-beta sweep, involves an angle-of-attack excursion from 3.0° to 40.0° and a simultaneous angle-of-sideslip excursion from 5.0° to -10.0° . Maneuver II was performed at an average Mach number of 0.6 and an average altitude of 9145 m (30,000 ft) (fig. 5).

PNEUMATIC LAG CORRECTIONS

The time lag values for each of the five pressure orifices on the test sensor were estimated using the previously described methods. To give a standard for comparison between maneuvers I and II, the estimated lags were extrapolated to sea level and zero

Mach number by the method of reference 7. The time lag values for both maneuvers are presented along with their uncertainty estimates (see app. 2) in table 2.

The uncertainty estimates for maneuver II are significantly higher than those for maneuver I. This most likely is due to the larger angle-of-sideslip excursions experienced during maneuver II. The asymmetric flows thus induced made the task of modeling the free-stream reference pressure at the orifice difficult; hence, the free-stream reference is believed to be less accurate for maneuver II (see app. 2). As an example, the test sensor raw and lag-corrected p_i ($i = 1$ to 5) time histories for maneuver I are presented in figure 6.

UPWASH CORRECTIONS

The estimated upwash adjustment factors are presented in table 3, along with the Yaggy-Rogallo estimates of the upwash adjustment factors. The Yaggy-Rogallo values were computed using the average Mach number for the respective maneuver. The aircraft wing sweep was set according to the schedule of the automatic flight control system at 49.0° for maneuver I and 22.0° for maneuver II. Yaggy-Rogallo calculations give upwash factors that are about 20 percent lower than the empirical estimates. Based upon previous experience, this agreement is within the expected accuracy of the Yaggy-Rogallo technique.

FLIGHT DATA RESULTS

The test sensor angle-of-attack data obtained from maneuver I were adjusted for lag and upwash. Time histories of the adjusted data are shown compared with the reference sensor data in figure 7. Figure 7(a) shows the time history for test sensor angle-of-attack data adjusted for lag only compared with the reference sensor angle-of-attack data. Figure 7(b) presents an analogous comparison with the test sensor data adjusted for upwash only. Finally, figure 7(c) presents the same comparison with the test sensor data adjusted for both lag and upwash. Although some discrepancy between the test sensor and reference sensor data is still present, the maximum discrepancy has been reduced from a nominal 10° to less than 2° .

The same analyses were performed on the maneuver II data (fig. 8). As before, the maximum difference between the test sensor and reference sensor data is reduced from approximately 10° to less than 2° .

The reasons for the remaining discrepancies have yet to be fully explained. The most likely explanation is that the simplified models used to describe lag and upwash on the test sensor do not fully describe the complex conditions that actually occur on the aircraft. The adjustments presented are not intended to be a calibration of the test sensor; instead, they are intended to offer a plausible explanation for the very large discrepancies between measurements of the two sensors..

CONCLUDING REMARKS

Wind tunnel data are presented to establish that the errors in the isolated hemispherical sensor measurements are significantly lower than the discrepancies as pre-

sented in reference 1. To examine plausible explanations for the data discrepancies, data obtained from the test sensor were adjusted for pneumatic lag and upwash. The adjustments were performed for two typical high-angle-of-attack maneuvers. The test sensor data corrected for lag and upwash were found to be in good agreement with the reference sensor data.

Because the high-angle-of-attack data investigated here were limited, there is still some question as to how large an angle-of-attack envelope can be reliably defined under maneuvering conditions. Further research is required to identify this envelope.

*National Aeronautics and Space Administration
Ames Research Center
Dryden Flight Research Facility
Edwards, California, July 14, 1986*

APPENDIX 1 - CONVERSION OF LAG DYNAMICS MODEL TO DIGITAL COMPENSATOR

As derived in reference 7, the lag model is approximately described by a non-linear, first-order differential equation,

$$\frac{dp(\ell, t)}{dt} + \frac{1}{\tau_a} p(\ell, t) = \frac{1}{\tau_a} p_t(t) \quad (3)$$

where

$$\tau_a = \frac{128\mu V \ell}{\pi D^4 p(\ell, t)}$$

D is the diameter of the pressure transmission line, $p_t(t)$ is the pressure at the free-stream end of the measurement device, V is the sensor configuration enclosed volume, and μ is the dynamic viscosity of air. This nonlinear equation is not amenable to analytic solution. However, if the magnitude of $p(\ell, t)$ changes by only a small amount during the maneuver, equation (3) may be integrated numerically to give the desired compensator. Assuming that the data are sampled at a constant regular interval Δt , equation (3) may be integrated from sample time $(k)\Delta t$ to sample time $(k+1)\Delta t$ by forward Euler integration to give

$$p(\ell, k+1) = \frac{\Delta t}{\tau_a} [p_t(k) - p(\ell, k)] + p(\ell, k)$$

and integrated from sample time $(k-1)\Delta t$ to sample time $(k)\Delta t$ by implicit Euler integration to give

$$p(\ell, k) = \frac{\Delta t}{\tau_a} [p_t(k) - p(\ell, k)] + p(\ell, k-1)$$

For simplicity of notation, the Δt following the sample index has been dropped. Superimposing the two solutions and solving for $p_t(k)$ gives the result

$$p_t(k) = \frac{\tau_a}{2(\Delta t)} [p(\ell, k+1) - p(\ell, k-1)] + p(\ell, k) \quad (4)$$

This is the final form of the digital compensator. Equation (4) approaches the exact solution as the sample interval of the system approaches zero. It provides a convenient method of reconstructing an unlagged pressure time history given the measured pressure time history. Several observations may be made with regard to equation (4):

1. The compensator is nonrecursive; that is, it is independent of previous values of $p_t(t)$. It is a finite impulse response filter, and as a result, it will introduce no phase changes in the data.
2. Because the compensator is symmetric in time, it cannot be implemented in real time.
3. The compensator acts as a high-frequency amplifier. As a result, high-frequency noise in the raw measurements may overwhelm the desired signal when equation (4) is applied. Care must be taken to insure that unwanted high-frequency elements are removed by prefiltering the raw data.

APPENDIX 2 — ESTIMATION OF LAG PARAMETERS

As mentioned in appendix 1, reference 7 shows that the lag dynamics model may be approximated by a first-order low-pass filter. The filter time lag value is a function of the measurement configuration geometry (that is, plumbing), dynamic viscosity, and pressure within the measurement device transmission line. For this report, we define the time lag values as being approximately described by

$$\tau_a = T_g \mu / p_t(t) \quad (5)$$

where T_g is an unknown lag geometry parameter still to be determined. This leads to the lag model that will be used,

$$\frac{dp(l, t)}{dt} + \frac{p_t(t)/\mu}{T_g} p(l, t) = \frac{p_t(t)/\mu}{T_g} \quad (6)$$

Flight test experience has shown that the geometry parameter T_g must be experimentally determined for each individual measurement configuration. The empirical technique to be used in estimating this parameter is the maximum likelihood technique.

Equation (6), which is being used to model the lag dynamics, is a bilinear, first-order, forced, ordinary differential equation with parameters that vary as functions of time. The exact values for the parameters of equation (6) are unknown. The system is excited by local pressures at the orifices, and the response, $p(l, t)$, is measured. Conceptually, the values of the unknown parameters may be inferred from the measured system response. Unfortunately, two complicating factors arise in practice. First, our knowledge of the form of the dynamic model is inherently imperfect, and second, a dynamic value for the input pressure at the sensor surface is not known. It is not possible to identify exactly the unknown parameters; rather, the values must be estimated by adherence to some statistical criterion. Such a criterion is the maximum likelihood criterion.

The maximum likelihood method consists of choosing a set of parameters (the most likely set) such that the dynamic model gives a response that is in close agreement with the measured response. This is accomplished by choosing the parameters such that they minimize the weighted sum of the squared differences between the measured system response and the response of the dynamic model when excited by the system input. An in-depth discussion of the maximum likelihood technique may be found in references 9 to 11. The modified maximum likelihood estimation program version 3 (MMLE3) is used to mechanize the actual estimation procedure. An in-depth discussion of MMLE3 may be found in references 11 and 12.

Cramér-Rao Bounds

With any parameter estimation method, it is important to have a measure of the accuracy of the estimates. Reference 5 discusses the evaluation of the accuracies, including a detailed treatment that is not given here. Therein, the Cramér-Rao bound is described as the best known analytical measure of the accuracy of maximum likelihood estimates. The Cramér-Rao bound gives a lowest limit on the variance of the estimate, and for large time intervals, this limit approaches the variance of the estimate. The Cramér-Rao bound was used to guide the iterative analysis described in

this appendix. The smaller the Cramér-Rao bound, the more confidence can be placed in the estimates. The square root of the Cramér-Rao bound is considered to be a practical estimate of the uncertainty (standard deviation) in the parameter estimate.

Estimation of the Input to the Sensor Configuration

As previously mentioned, the pressure at the surface of the sensor is not directly available and must be estimated from alternative data sources. There is no clearly optimal method that can be used to accomplish this task. The following method was chosen to estimate this pressure.

First, a time history for the free-stream dynamic pressure q is estimated using the linearized Kalman filter technique, described in detail in appendix 3. This time history contains high-frequency information that is representative of the high-frequency content of the pressure at the sensor surface. The low-frequency components of the q estimate are stripped away using a high-pass digital filter.

Second, the measured pressure time history, $p(\ell, t)$ is passed through a low-pass digital filter with the same rolloff, damping, and order as the high-pass filter. This strips off the high-frequency information while retaining the low-frequency components, which are not greatly affected by pneumatic lag.

Third, the low-pass- and high-pass-filtered data are summed to give a composite signal, $p_c(t)$, which is a rough estimate of $p_t(t)$. To account for additional scaling and bias terms, a scale factor F and a bias term b are included so that

$$p_t(t) = F p_c(t) + b$$

The values for F and b may either be estimated by the maximum likelihood technique as a part of the identification loop or be chosen by engineering judgment. For the present study, the values of F and b were chosen by engineering judgment; that is, the values of F and b were chosen so as to give a good data fit while still keeping the Cramér-Rao bounds low. The values for F and b for the two maneuvers are presented in table 4

This approach is referred to as a complementary filter (ref. 12). The complementary filter concept is illustrated in figure 9, which shows the magnitude plots of both the low-pass and the high-pass filters (fig. 9(a)) and the information flow of the complementary filtering process (fig. 9(b)). The low-frequency components of the linearized Kalman filter dynamic pressure (q_{LKf}) are removed, and the high-frequency components of the measured response are removed. The resulting summation superimposes the high-frequency linearized Kalman filter signal on the measured response.

In summary the following identification scheme was used to estimate T_g :

1. Calculate p_c by the complementary filter process.
2. Choose or estimate the scale factor F and bias term b .
3. Choose a starting value for T_g .
4. Use MMLE3 to estimate the most likely value of T_g given p_c , F , and b .

5. Compute the predicted model response for $p(\ell, t)$
6. Compute the weighted error sum (maximum likelihood cost), and adjust the value of the unknown parameter T_g , by the maximum likelihood criterion.
7. Iterate steps 4 to 7 until the maximum likelihood cost reaches a minimum.

The estimation of the value of T_g completes the design of our digital compensator.

APPENDIX 3 — COMPUTATION OF FREE-STREAM AIR DATA PARAMETERS
BY THE LINEARIZED KALMAN FILTER TECHNIQUE

The techniques for estimating the adjustment factors utilize a high-frequency, highly accurate set of air data parameters that were derived by merging several data sources using a linearized Kalman filter. This technique provided an independent set of parameters that were not strongly affected by upwash, position, and lag errors. This appendix briefly describes the linearized Kalman filter technique and the data sources that were merged. An in-depth discussion of the technique may be found in reference 13.

Description of Data Sources

Data from both onboard and external sources were used to reconstruct air data time histories for maneuvers I and II. The onboard sources were body axis linear accelerations and rotational rates, pitot-static measurements from the air inlet control system (AICS) probe, and flow angle data from the reference air data probes. The external sources were C-band tracking data and upper-atmosphere data from meteorological analyses.

The strap-down linear accelerometer data provided three-axis accelerations and were corrected for center-of-gravity offsets using the rotational rate measurements. The accelerometer data had a flat frequency response in excess of 20 Hz.

The pitot-static data were provided by two AICS side-mounted hemispherical sensors. These data, once corrected for position error, provided rough estimates of free-stream static and dynamic pressures. These data had a flat frequency response on the order of 10 Hz.

The radar tracking data provided three-axis position and velocity data and estimates of flightpath angle and heading. The velocity and direction angles, because they are the result of differentiated position data, are naturally unbiased. The sampling rate of these data is 20 samples/sec. The flat frequency response of the data is on the order of 10 Hz.

Upper-atmosphere meteorological quantities resulting from analyses of rawinsonde balloon data provided low-frequency estimates of ambient pressure, ambient temperature, and winds aloft. These data represent a time-averaged value for the parameters discussed. The upper-atmospheric analyses are described in depth in reference 13.

Merging of Multiple Data Sources

The data sources were combined by the linearized Kalman filter in a manner that superimposed the high-frequency data on the low-frequency data. Biases and systematic errors were identified by redundant information contained in the various data sources. The resulting time history values for airspeed, groundspeed, angle of attack, angle of sideslip, heading angle, flightpath angle, dynamic pressure, and static pressure have very low bias and a flat frequency response on the order of 10 Hz. Further information concerning this technique may be found in references 12 and 13.

REFERENCES

1. Larson, Terry J.: Evaluation of a Flow Direction Probe and a Pitot-Static Probe on the F-14 Airplane at High Angles of Attack and Sideslip. NASA TM-84911, 1984.
2. Montoya, Earl J.: Wind-Tunnel Calibration and Requirements for In-Flight Use of Fixed Hemispherical Head Angle-of-Attack and Angle-of-Sideslip Sensors. NASA TN D-6986, 1973.
3. Bennett, Donald L.: Evaluation of a Hemispherical Head Flow Direction Sensor for Inlet Duct Measurements. NASA TM X-3232, 1975.
4. Armistead, Katherine H.; and Webb, Lannie D.: Flight Calibration Tests of a Nose-Boom-Mounted Fixed Hemispherical Flow-Direction Sensor. NASA TN D-7461, 1973.
5. Gilyard, Glenn B.; and Belte, Daumants: Flight-Determined Lag in Angle-of-Attack and Angle-of-Sideslip Sensors in the YF-12A Airplane from Analysis of Dynamic Maneuvers. NASA TN D-7819, 1974.
6. Hagen, Floyd W.; and DeLeo, Richard V.: Wind Tunnel Evaluation of a Flow Direction Probe and a Pitot-Static Probe for Use on F-14 Aircraft. Rosemount Corporation Report D8400295, Minneapolis, Minnesota, Nov. 1984.
7. Lamb, J.P., Jr.: The Influence of Geometry Parameters Upon Lag Error in Airborne Pressure Measuring Systems. WADC TR-57-351, July 1957.
8. Rawlings, Kenneth, III: A Method of Estimating Upwash Angle at Noseboom-Mounted Vanes. AFFTC-TIM-81-1, June 1981.
9. Hagen, Floyd W.; and DeLeo, Richard V: Wind Tunnel Calibration of a Flow Direction Sensor and a Pitot-Static Tube to High Angles of Attack and Sideslip. Proc. IEEE National Aerospace and Electronics Conference, Dayton, Ohio, May 1985.
10. Goodwin, Graham C.; and Payne, Robert L.: Dynamic System Identification: Experiment Design and Data Analysis. Academic Press, New York, 1977.
11. Maine, Richard E.: Programmer's Manual For MMLE3, A General FORTRAN Program for Maximum Likelihood Parameter Estimation. NASA TP-1690, 1981.
12. Maine, Richard E.; and Iliff, Kenneth W.: User's Manual for MMLE3, A General FORTRAN Program for Maximum Likelihood Parameter Estimation. NASA TP-1563, 1980.
13. Whitmore, Stephen A.: Formulation and Implementation of Nonstationary Adaptive Estimation Algorithm With Applications to Air-Data Reconstruction. NASA TM-86727, 1985.
14. Whitmore, Stephen A.; Larson, Terry J.; and Ehernberger, L.J.: Air Data Position-Error Calibration Using State Reconstruction Techniques. NASA TM-86029, 1984.

TABLE 1. - WIND TUNNEL TEST CONDITIONS

Mach number	Angle of sideslip, deg	Angle of attack, deg
0.3	0	-4.0 to 60.0
0.4	0	-4.0 to 60.0
0.5	0	-4.0 to 60.0
0.3	-30.0 to 30.0	0
0.3	-30.0 to 30.0	7.0

TABLE 2. - NORMALIZED SEA LEVEL TIME LAG VALUES AND UNCERTAINTY ESTIMATES FOR TEST SENSOR PRESSURE DATA

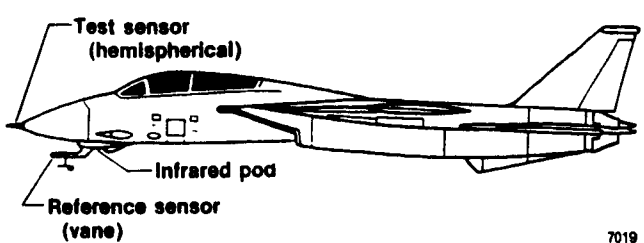
Pressure orifice	Maneuver I		Maneuver II	
	Lag, msec	Uncertainty, msec	Lag, msec	Uncertainty, msec
P1	125	15.4	133	38.6
P2	125	16.1	133	39.5
P3	122	27.4	139	44.2
P4	122	27.6	139	43.4
P5	159	19.4	158	41.4

TABLE 3. - UPWASH ADJUSTMENT FACTORS FOR TEST SENSOR

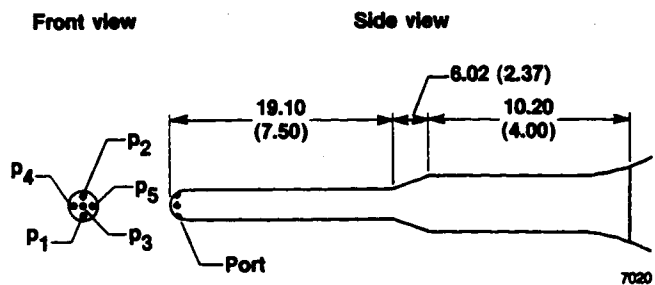
Factor	Maneuver I	Maneuver II
Estimated upwash	0.142	0.330
Yaggy-Rogallo upwash	0.1202	0.273

TABLE 4. - VALUES OF SCALING AND BIAS TERMS FOR INPUT PRESSURE

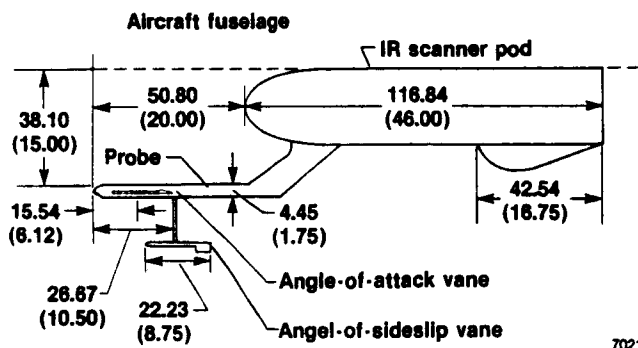
	Scale factor F	Bias term b, kPa (lb/ft ²)
Maneuver I	1.15	0.239 (5.0)
Maneuver II	1.08	0.302 (6.3)



(a) Air data sensor locations.



(b) Test probe orifice locations and notation.



(c) Reference probe.

Figure 1. Sensors used in high-angle-of-attack flight tests.

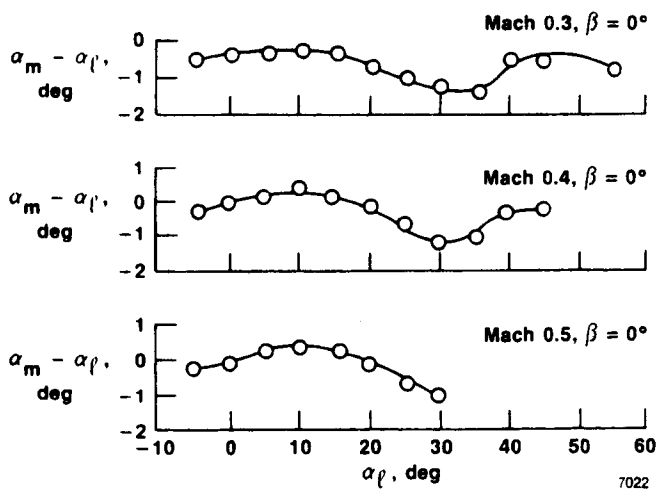


Figure 2. Wind tunnel angle-of-attack calibration for isolated test sensor as a function of angle of attack.

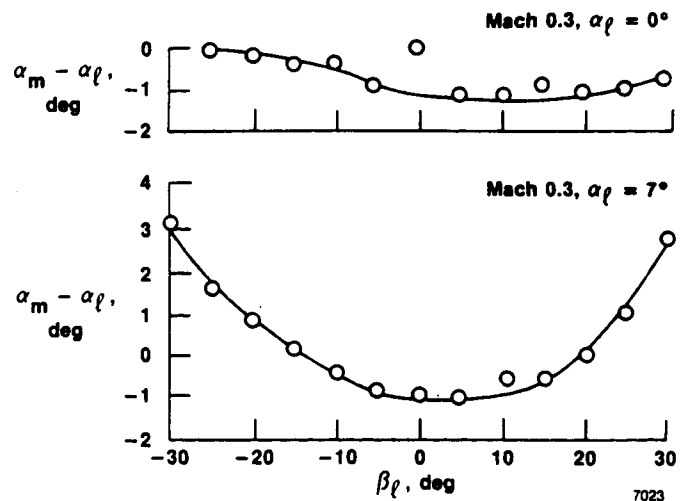


Figure 3. Wind tunnel angle-of-attack calibration for test sensor as a function of angle of sideslip.

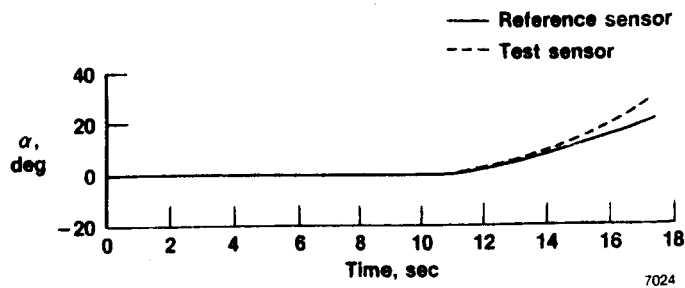


Figure 4. Angle-of-attack comparison, maneuver I.

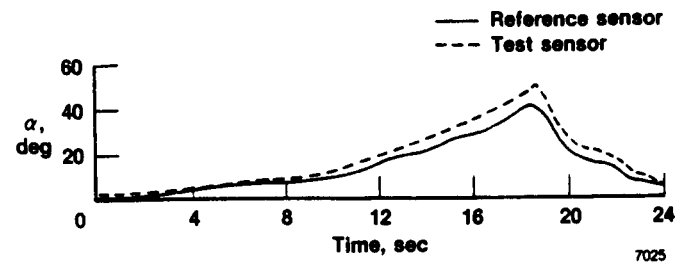


Figure 5. Angle-of-attack comparison, maneuver II.

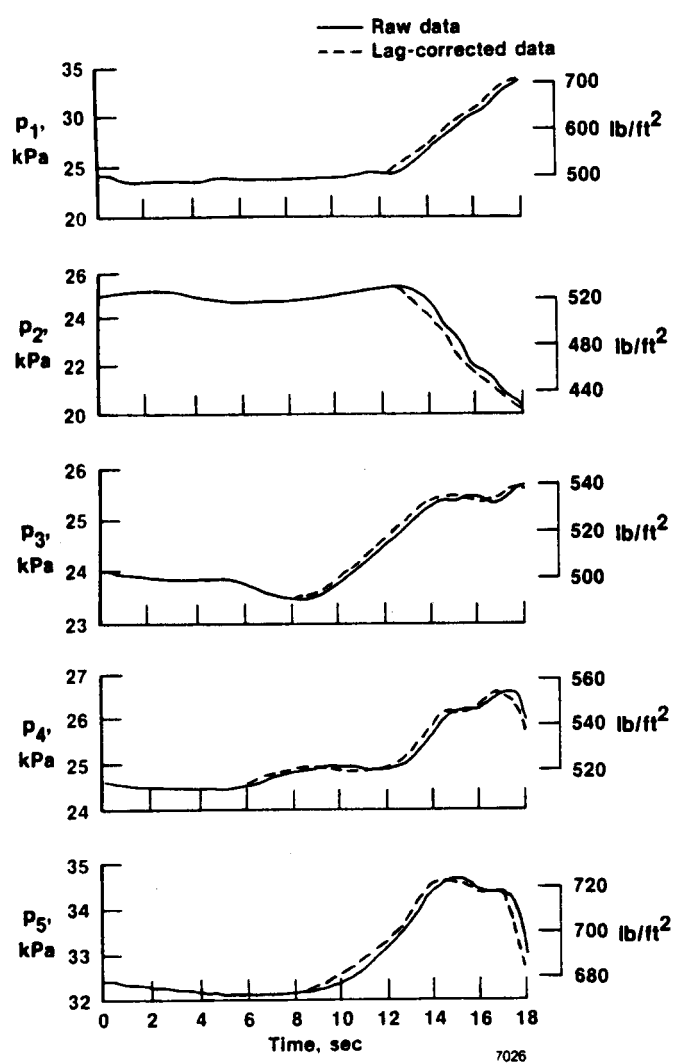


Figure 6. Time history comparison of raw and lag-corrected test probe pressure data, maneuver I.

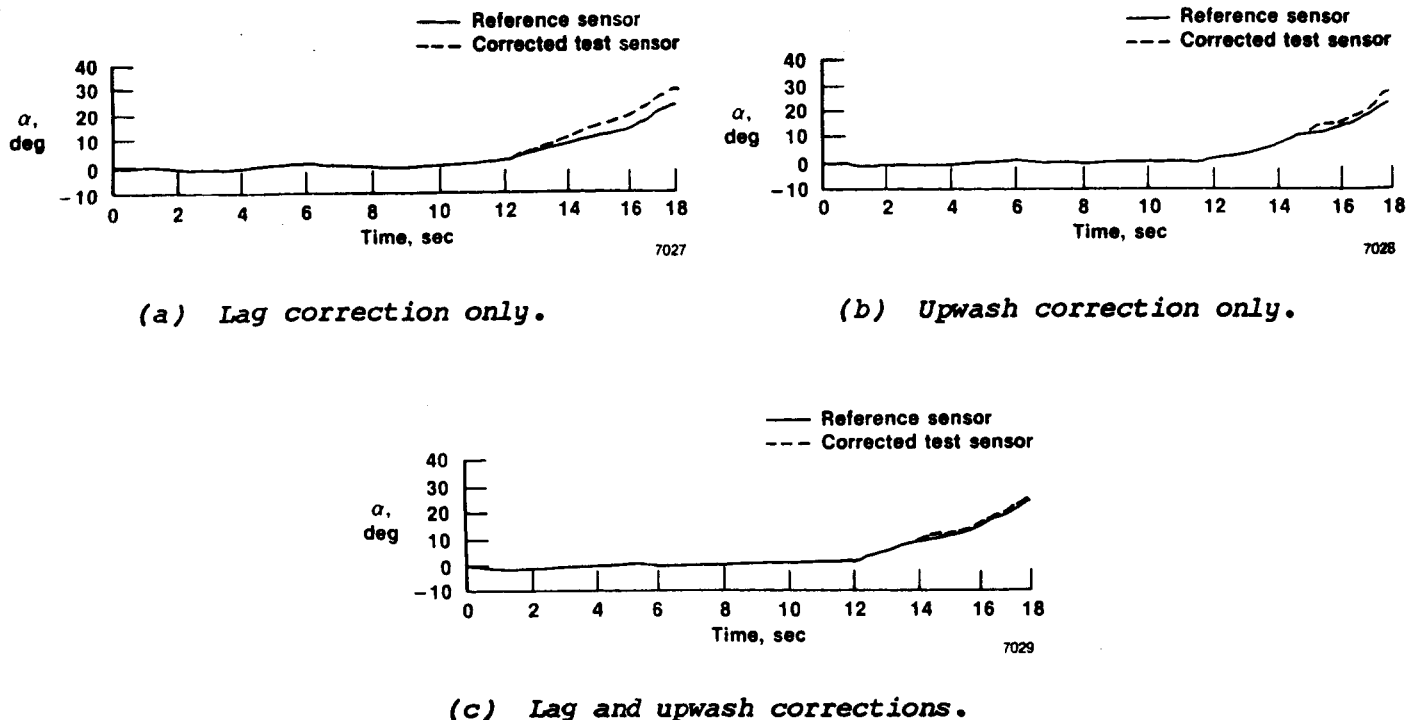


Figure 7. Angle-of-attack time history comparisons, maneuver I.

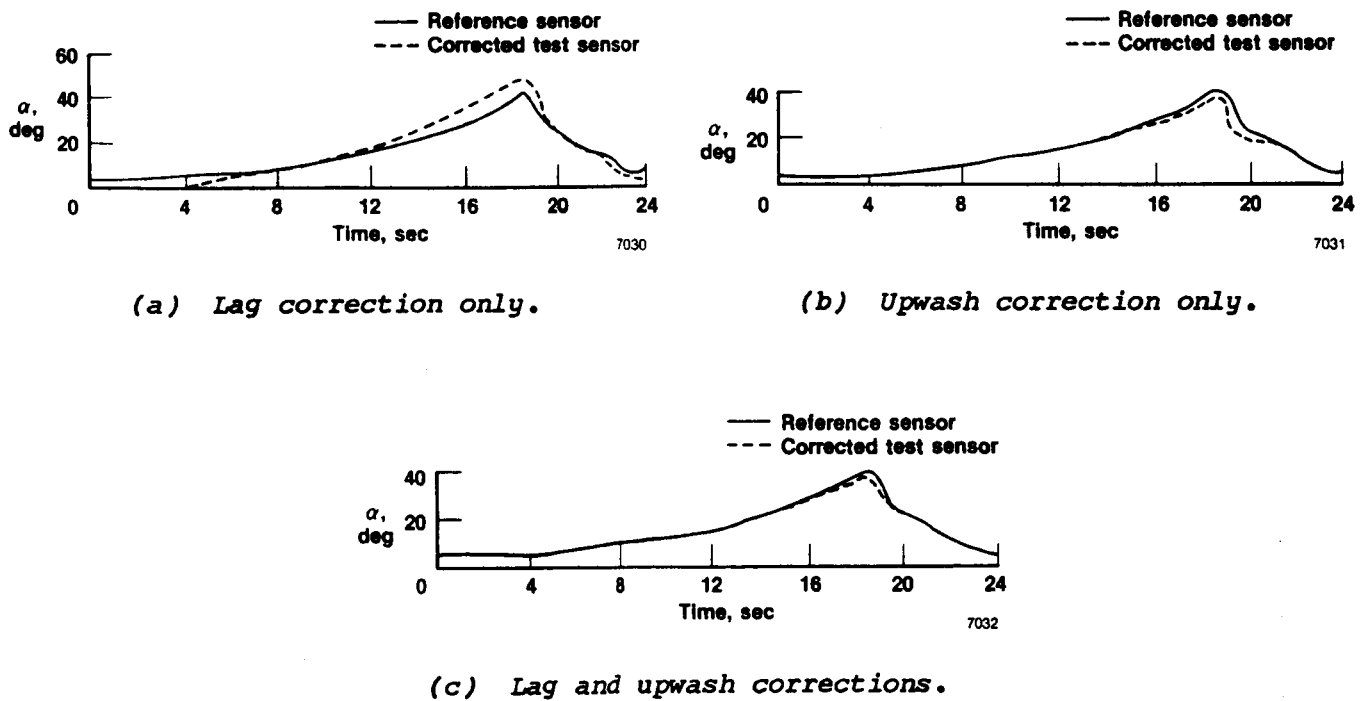
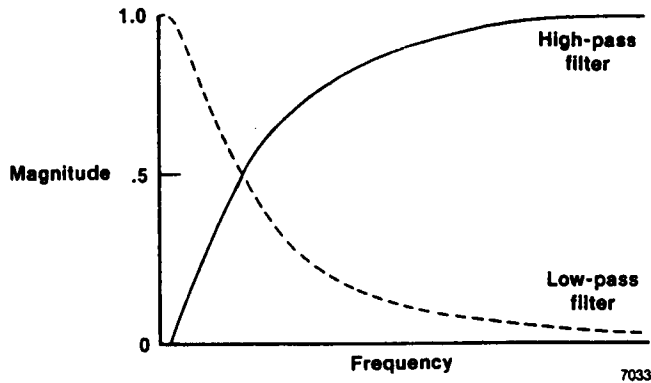
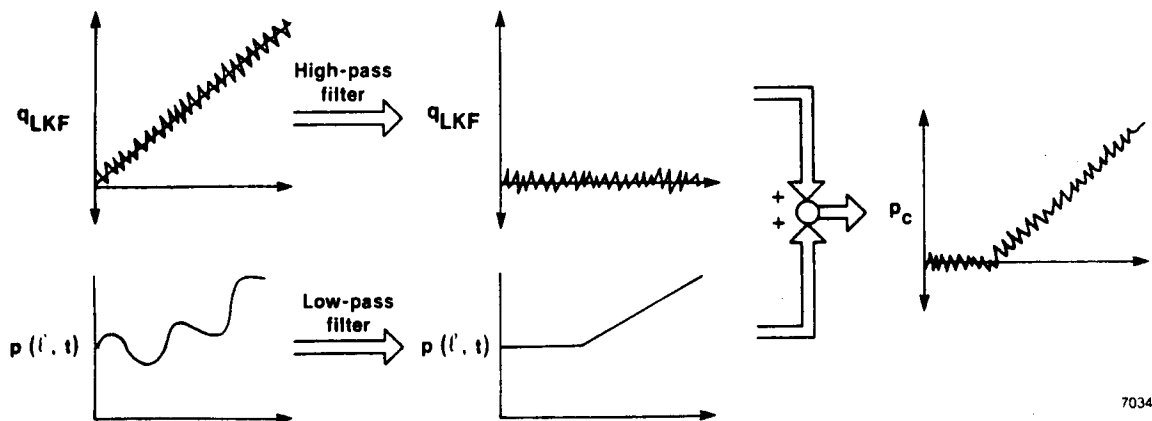


Figure 8. Angle-of-attack time history comparisons, maneuver II.



(a) Magnitude plot.



(b) Information flow.

Figure 9. Complementary filter concept for estimating local pressure at the test sensor surface.

1. Report No. NASA TM-86790	2. Government Accession No.	3. Recipient's Catalog No.	
4. Title and Subtitle High-Angle-of-Attack Pneumatic Lag and Upwash Corrections for a Hemispherical Flow Direction Sensor		5. Report Date May 1987	
		6. Performing Organization Code	
7. Author(s) Stephen A. Whitmore, Jennifer Heeg, Terry J. Larson, L.J. Ehernberger, Floyd W. Hagen, and Richard. V. DeLeo		8. Performing Organization Report No. H-1314	
9. Performing Organization Name and Address NASA Ames Research Center Dryden Flight Research Facility P.O. Box 273 Edwards, CA 93523-5000		10. Work Unit No. RTOP 505-43-31	
		11. Contract or Grant No.	
12. Sponsoring Agency Name and Address National Aeronautics and Space Administration Washington, DC 20546		13. Type of Report and Period Covered Technical Memorandum	
		14. Sponsoring Agency Code	
15. Supplementary Notes Floyd W. Hagen and Richard V. DeLeo are affiliated with Rosemount, Inc., Eden Prairie, Minnesota			
16. Abstract			
<p>As a part of the NASA F-14 high-angle-of-attack flight test program, a nose-mounted hemispherical flow direction sensor was calibrated against a fuselage-mounted movable-vane flow angle sensor. Significant discrepancies were found to exist in the angle-of-attack measurements.</p> <p>This report describes a two-fold approach taken to resolve these discrepancies during subsonic flight. First, the sensing integrity of the isolated hemispherical sensor is established by wind tunnel data extending to an angle of attack of 60°. Second, two probable causes for the discrepancies, pneumatic lag and upwash, are examined. Methods of identifying and compensating for lag and upwash are presented.</p> <p>The wind tunnel data verify that the isolated hemispherical sensor is sufficiently accurate for static conditions with angles of attack up to 60° and angles of sideslip up to 30°. Analysis of flight data for two high-angle-of-attack maneuvers establishes that pneumatic lag and upwash are highly correlated with the discrepancies between the hemispherical and vane-type sensor measurements.</p>			
17. Key Words (Suggested by Author(s)) Hemispherical sensor High angle of attack Pneumatic lag Upwash		18. Distribution Statement Unclassified — Unlimited Subject category 06	
19. Security Classif. (of this report) Unclassified	20. Security Classif. (of this page) Unclassified	21. No. of Pages 19	22. Price* A02

*For sale by the National Technical Information Service, Springfield, Virginia 22161.